Coulomb excitation of ^{96}Mo

R. Russell,[1,*] J. Heery,[1] J. Henderson,[1] C. R. Hoffman,[2] T. Beck,[4] C. Cousins,[1] P. Farris,[3,4] A. Gade,[3,4] S. A. Gillespie,[4] A. Hill,[3] H. Iwasaki,[3,4] S. Kisyov,[5,†] A. N. Kuchera,[6] B. Longfellow,[5] C. Müller-Gatermann,[2] K. Nomura,[7] E. Rubino,[3,‡] R. Salinas,[3,4] A. Sanchez,[3,4] D. Weisshaar,[4] C. Y. Wu,[5] and J. Wu[4,§]

[1]*School of Maths and Physics, University of Surrey, Guildford, GU2 7XH Surrey, United Kingdom*
[2]*Physics Division, Argonne National Laboratory, Lemont, Illinois 60439, USA*
[3]*Department of Physics and Astronomy, Michigan State University, East Lansing, Michigan 48824, USA*
[4]*Facility for Rare Isotope Beams, Michigan State University, East Lansing, Michigan 48824, USA*
[5]*Lawrence Livermore National Laboratory, Livermore, California 94550, USA*
[6]*Department of Physics, Davidson College, Davidson, North Carolina 28035, USA*
[7]*Department of Physics, Hokkaido University, Sapporo 060-0810, Japan*

(Received 8 September 2023; accepted 6 December 2023; published 19 December 2023)

The neutron-rich strontium, zirconium, and molybdenum nuclei have been observed to undergo a dramatic evolution, becoming strongly deformed around $N = 60$, sometimes interpreted as a quantum phase transition between "normal" and intruder configurations. Key to understanding this evolution is to understand the configurations in isolation, in regions where interference can be neglected. A deformed coexisting configuration is inferred from the presence of a 0_2^+ state which decreases in excitation energy with increasing neutron number, becoming the first-excited state at ^{98}Mo. We present here the results of a low-energy Coulomb-excitation measurement of the nucleus ^{96}Mo, extracting $B(E2)$ values and quadrupole moments. It is found that, while the $B(E2)$ values agree with those found in the literature, there is a significant disagreement with literature spectroscopic quadrupole moments. The results are compared with shell-model calculations using a ^{88}Sr core with good agreement found, likely indicating that intruder structures do not significantly impact the ground-state structure, in contrast with the heavier molybdenum isotopes.

DOI: 10.1103/PhysRevC.108.064311

I. INTRODUCTION

A key understanding in nuclear physics is that most atomic nuclei possess some form of deformation in their intrinsic frame. The most commonly observed nuclear shape is $L = 2$ (quadrupole) which is ubiquitous across the nuclear chart and leads to collective excitations which are quite different to those predicted by purely independent-particle theories.

It is generally understood that the nucleon-nucleon (NN) interaction employed in the nuclear shell model gives rise to collective correlations due to strong configuration mixing [1]. This mixing occurs for "valence" nucleons in single-particle orbits on top of the appropriate closed proton and neutron shell (inert core). The emergence of quadrupole deformation is driven by the quadrupole component of the NN interaction. In the cases where nuclear shells are filled, around magic numbers, spherical or near-spherical configurations are dominant due to the large energy gap between the core and the valence space. In midshell regions, quadrupole-quadrupole (QQ) correlations are increased leading to large quadrupole deformation. In between there are transitional regions where shape changes occur, sometimes in the space of only a few nuclei.

At $N = 60$, it has been observed that strontium, zirconium, and molybdenum isotopes undergo a dramatic change in nuclear shape. This rapid change is due to the energetically favorable conditions of deformed intruder orbitals, which are driven down in energy by QQ correlations [2]. Previous work has shown that ^{92}Mo$_{50}$ is spherical in its ground state due to the $N = 50$ shell closure [3]. The addition of neutrons beyond $N = 50$ leads to a gradual increase in deformation until ^{102}Mo$_{60}$ where a sudden increase occurs [4]. In contrast to ^{98}Mo, where the 0_2^+ state becomes the first-excited state, and ^{100}Mo, where a dramatic reduction in 2_1^+ energy is observed, the energy and $E2$ excitation strength of the 2_1^+ state in ^{96}Mo do not show obvious signatures of perturbation. It is therefore important for constraining theoretical models by verifying whether this unperturbed hypothesis holds.

*reuben.russell@surrey.ac.uk
†Present address: Accelerator Technology and Applied Physics Division, Lawrence Berkeley National Laboratory, Berkeley, California 94720, USA.
‡Present address: Lawrence Livermore National Laboratory, Livermore, California 94550, USA.
§Present address: National Nuclear Data Center, Brookhaven National Laboratory, Upton, New York 11973, USA.

Previous work on ^{96}Mo has been carried out by Paradis *et al.* in 1976 [5], and Barrette *et al.* in 1971 [6]. Both these previous studies and this work have utilized Coulomb excitation for the measurement of the shape properties in ^{96}Mo. Previous work used low-Z probes, which are less sensitive to higher-order effects such as multistep excitations and the re-orientation effect. In this work we present Coulomb excitation of a ^{96}Mo beam on a ^{196}Pt target, providing enhanced sensitivity to these higher-order effects.

II. EXPERIMENTAL METHODS

The experiment was carried out at the National Superconducting Cyclotron Laboratory (NSCL) with use of the reaccelerated beam facility (ReA6) on site. A sample of ^{32}Si was ionised and introduced to ReA6 where it was accelerated to 3.57 MeV/u. The primary contaminant in this beam was ^{96}Mo, which made up ∼10% of the beam and is the subject of the present work. The beam was impinged upon a 1.59 mg/cm^2 ^{196}Pt target, with a ∼2.5% ^{194}Pt impurity, mounted inside the Joint Arrays For Nuclear Structure (JANUS) setup [7]. The JANUS setup comprises the Segmented Germanium Array (SeGA) [8] in a barrel configuration around S3-type annular silicon particle detectors up and down stream from the target. The data from the upstream detector are not used for this work given that the statistics were too low to allow for reliable analysis. The laboratory frame angular coverage provided by the downstream S3 detector is 21.9°–52.0°. This experiment satisfies the 5 fm distance Cline criterion for safe Coulomb excitation since the minimum impact parameter for these nuclei is $\geqslant$ 7.5 fm [9–11].

Excited states in both ^{96}Mo and ^{196}Pt nuclei were populated via the Coulomb force between them. Scattered nuclei were detected in the S3 detectors, whilst prompt γ rays, emitted in the de-excitation of the populated excited states, were detected in SeGA. The ^{96}Mo nuclei strike the target at an energy which is ∼88% of the Coulomb barrier. The nuclei therefore remained beyond the range of the strong nuclear force and only electromagnetic interactions make a significant contribution to the excitation process. The digital data acquisition system used was comprised of 100 MHz and 250 MHz XIA Pixie-16 modules for SeGA and the S3 detectors, respectively, running in a triggerless continuous-running mode. The data were analyzed using the GRUTINIZER [12] software package built in a ROOT [13] framework. Further data analysis used the JROOT [14] software package.

Scattered particles detected in the downstream S3 detector can be seen in Fig. 1, where ring number relates to the angle at which the particle was detected. Kinematic lines in Fig. 1 relating to the different projectiles detected can be clearly distinguished from one another. Analysis of the ^{32}Si is the subject of a separate publication [15].

γ rays detected by SeGA were Doppler corrected with respect to the corresponding particle's reaction kinematics and the detected angles of the recoiled particles. Figure 2 contains Doppler corrected γ-ray spectra for ^{96}Mo and ^{196}Pt. The γ rays seen in Fig. 2 for ^{96}Mo are the 778 keV ($2_1^+ \rightarrow 0_1^+$) and 850 keV ($4_1^+ \rightarrow 2_1^+$). For ^{196}Pt the transitions observed are the 356 keV ($2_1^+ \rightarrow 0_1^+$) and the 521 keV ($4_1^+ \rightarrow 2_1^+$). A transition

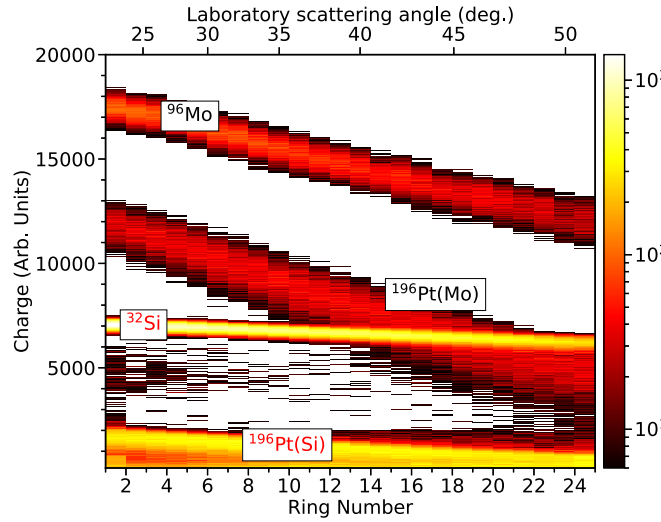

FIG. 1. Charge detected in the rings of the downstream S3 detector. The laboratory angles are shown on the upper axis. The top band is the ^{96}Mo scattered by the ^{196}Pt in the target, the second band is the ^{196}Pt which is scattered by the ^{96}Mo in the beam. Additionally, ^{32}Si and the corresponding ^{196}Pt are seen due to the ^{32}Si nuclei being the primary components in the beam. Note that bins containing less than five counts have been omitted from this figure for the purposes of presentation.

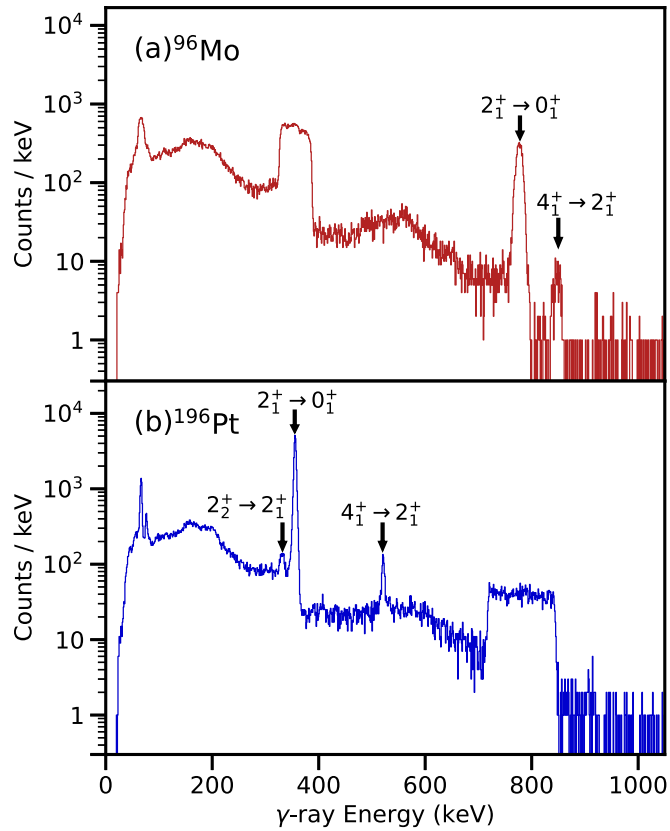

FIG. 2. Doppler corrected γ-ray spectra for ^{96}Mo (a) and ^{196}Pt (b) obtained with SeGA. When correcting for the Mo recoils two peaks can be seen; 778 keV and 850 keV. Similarly for Pt three peaks are seen; 333 keV, 356 keV, and 521 keV.

TABLE I. Table for the literature values of the matrix elements used for ^{196}Pt in GOSIA [11,19,20].

J_i^π	J_f^π	$\langle J_i^\pi \mid E2 \mid J_f^\pi \rangle$ [e^{2}b^2]	$\langle J_i^\pi \mid M1 \mid J_f^\pi \rangle$ [μ_N]
0_1^+	2_1^+	1.172(5)	
2_1^+	2_1^+	0.82(10)	
2_1^+	2_2^+	1.36(1)	0.0723(64)
2_1^+	4_1^+	1.91(2)	
2_1^+	0_2^+	0.167(15)	
2_2^+	2_2^+	−0.52(20)	
2_2^+	0_2^+	−0.35(70)	
4_1^+	4_1^+	1.36(16)	

at 333 keV corresponding to the $2_2^+ \rightarrow 2_1^+$ in ^{196}Pt is seen but has not been included in the Coulomb excitation analysis due to a similar energy known for the $2_1^+ \rightarrow 0_1^+$ transition in ^{194}Pt. Excitation of ^{96}Mo by ^{194}Pt has also been accounted for in the analysis.

The yields from the Coulomb excitation were evaluated using the semiclassical coupled channels Coulomb excitation code GOSIA [16]. Use of the SRIM [17] software package was employed to account for energy loss of ions in the target to enable accurate inputs to GOSIA. An external χ^2 minimization was used, in conjunction with GOSIA, which uses the ROOT MINUIT libraries [18]. For the beam-like scattered particles, the data in center-of-mass (c.m.) angles ∼32°–75° were separated into three angular ranges in the downstream S3. In the case of the target-like scattered particles, a single angular range between c.m. angles ∼116°–136° avoiding contamination from ^{32}Si. The minimization was simultaneously carried out for ^{96}Mo and ^{196}Pt matrix elements, eliminating the need for internal normalisation and giving absolute sensitivity to $B(E2)$. The use of a single, high-Z target, provides good sensitivity to quadrupole moments and low-lying matrix elements, while the well-studied nature of ^{196}Pt ensures minimal systematic uncertainties arise from the target matrix elements. The literature values for the ^{196}Pt were gathered from Refs. [11,19,20], see Table I. Following the minimization, $E2$ matrix elements were extracted for the observed transitions in ^{96}Mo.

III. RESULTS

Important to Coulomb excitation are the effects of multistep excitations which cause interference, depending on the relative signs of the matrix elements involved, see Fig. 3. In this work, the excitation to the 2_1^+ state is a single-step process and interference comes primarily from the second and third 2^+ states. The probability of the 2_1^+ state being populated is proportional to the square of the excitation amplitudes while the interference can be simplified to constructive (+) or destructive (−) depending on the relative signs, where the signs are commonly referred to as P_3 [21].

The two dominant sources of interference are the 2_2^+ and 2_3^+ which have four possible P_3 combinations; $++, +-, -+, --$. A P_3 of $++$ would mean maximum

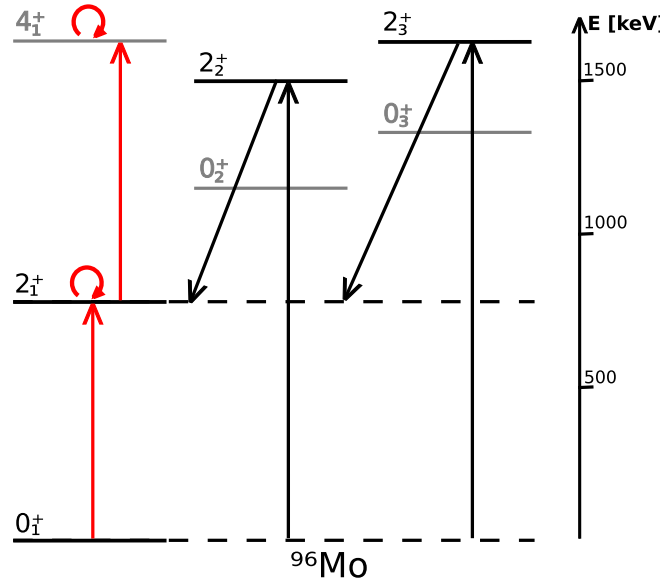

FIG. 3. A schematic view of levels and associated one- and two-step excitations and de-excitations. Where red arrows indicate those observed in this work and black arrows indicate literature values from Ref. [20] used to account for intruder states.

constructive interference, and $--$ therefore is maximum destructive interference. In this work there was not sufficient sensitivity to P_3 signs, so all combinations and the corresponding matrix elements have been presented in Table II. Analogous interference terms also exist for the 4_1^+ state, however, there is insufficient literature information to reliably constrain their contributions which are expected to be comparable to the statistical uncertainty in the quadrupole moment.

Confidence intervals for the $\langle 0_1^+ \mid E2 \mid 2_1^+ \rangle$ and $\langle 2_1^+ \mid E2 \mid 2_1^+ \rangle$ matrix elements are shown in Fig. 4, where the ellipses show the 1σ confidence. For the cases where $P_3 = ++$ and $--$, the χ^2 surfaces can be seen. A comparison between this work and the previous study of ^{96}Mo, Ref. [5], can be seen in Table II. Values for $\langle 0_1^+ \mid E2 \mid 2_1^+ \rangle$ matrix elements are all consistent and have only a small uncertainty. On the other hand, the $\langle 2_1^+ \mid E2 \mid 2_1^+ \rangle$ matrix elements have a large spread and a strong dependence on P_3. The $Q_s(2_1^+)$ values extracted in this work are inconsistent with those of Paradis *et al.* [5], with this work having larger and more negative $Q_s(2_1^+)$ values.

With regards to Ref. [5], since the $B(E2)$ from this work match well, the comparisons can be limited to the $Q_s(2_1^+)$ only. The $Q_s(2_1^+)$ values obtained in this work differ greatly from the previous work in Ref. [5] while still leaning towards a prolate deformation. When taking into account the interference caused by intruder states, see Table II, $Q_s(2_1^+)$ in this work varies between $-0.53\,(9)\,e$b and $-0.28\,(9)\,e$b. Whereas the work by Paradis *et al.* [5], under the same influences, has $Q_s(2_1^+)$ vary between $-0.20\,(8)$ eb and $+0.04\,(8)$ eb.

The $B(E2; 2_1^+ \rightarrow 4_1^+) = 2400\,(500)\,e^2\text{fm}^4$ measured in this work has only once before been measured, in Ref. [6], with $B(E2; 2_1^+ \rightarrow 4_1^+) = 1900\,(360)\,e^2\text{fm}^4$, agreeing with the present work within uncertainties. The $Q_s(4_1^+) = -0.3\,(4)\,e$b

TABLE II. Table containing matrix elements, $B(E2)$, and Q_s measurements when accounting for interference from intruder states. There is little difference between this work and Ref. [5] with regards to $B(E2)$ and significant differences for values of the Q_s while maintaining a similar trend along the results as P_3 is altered. The uncertainties quoted in these results are purely statistical, systematic error from the semiclassical GOSIA code is in the region of 3%.

$J_i^\pi \rightarrow J_f^\pi$	P_3		$\langle J_i^\pi \mid E2 \mid J_f^\pi \rangle$ [eb]	$B(E2; J_i^\pi \rightarrow J_f^\pi)$ [e^2fm^4] (This work)	$B(E2; J_i^\pi \rightarrow J_f^\pi)$ [e^2fm^4] (Previous work)
$0_1^+ \rightarrow 2_1^+$	+	+	0.519 (10)	2700 (100)	2710 (40)[a]
$0_1^+ \rightarrow 2_1^+$	+	−	0.519 (10)	2700 (100)	2700 (40)[a]
$0_1^+ \rightarrow 2_1^+$	−	+	0.518 (10)	2690 (100)	2700 (40)[a]
$0_1^+ \rightarrow 2_1^+$	−	−	0.519 (10)	2700 (100)	2690 (40)[a]
$2_1^+ \rightarrow 4_1^+$			1.10 (10)	2400 (500)	1900 (360)[b]
J_i^π	P_3		$\langle J_i^\pi \mid E2 \mid J_i^\pi \rangle$ [eb]	$Q_s(J_i^\pi)$ [eb] (This work)	$Q_s(J_i^\pi)$ [eb] (Previous work)
2_1^+	+	+	−0.69 (11)	−0.53 (9)	−0.20 (8)[a]
2_1^+	+	−	−0.59 (11)	−0.45 (9)	−0.15 (8)[a]
2_1^+	−	+	−0.46 (11)	−0.35 (9)	−0.01 (8)[a]
2_1^+	−	−	−0.36 (11)	−0.28 (9)	+0.04 (8)[a]
4_1^+			−0.3 (6)	−0.3 (4)	

[a]Paradis *et al.* 1976 [5].
[b]Barrette *et al.* 1971 [6].

extracted in this work is the first measurement for this quantity.

IV. DISCUSSION

A comparison between experimental results presented in this work, literature values, and shell-model calculations can be seen in Fig. 5. The shell-model predictions featured in Fig. 5 were obtained through use of the jj45a interaction in KSHELL [22] with a $\pi(p3/2, g9/2)\nu(g7/2, d5/2, d3/2, s1/2)$ valence space and effective charges of $e_\pi = 1.6$ and $e_\nu = 1.0$ [23]. Also shown for ^{96,98}Mo are calculations performed using an IBM-2 Hamiltonian mapped to a microscopic mean-field potential energy surface (PES). The PES is obtained through Hartree-Fock-BCS calculations using the Skyrme energy density functional and SLy6 interaction. Details of the calculations can be found in Ref. [24]. A ^{90}Zr inert core is assumed in the IBM-2 Hamiltonian with effective proton and neutron boson charges chosen to obtain good agreement with the experimental $B(E2; 0_1^+ \rightarrow 2_1^+)$ from ENSDF. The calculations are capable of including the mixing between different configurations arising from different intrinsic shapes.

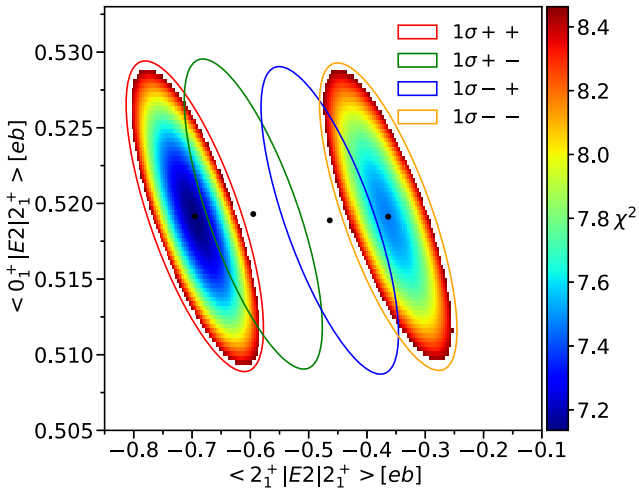

FIG. 4. Figure displaying confidence in the matrix elements in this work, as seen in Table II. The points in the center of each ellipse correspond to the matrix elements linked to respective P_3 + +, + −, − +, − −. The solid lines correspond to one standard deviation. For the ++ and −− configurations, the χ^2 surface is shown, cut off at the 1σ limit for both surfaces. The number of degrees of freedom was 22 in the fit, including both experimental data and literature constraints on ^{196}Pt matrix elements.

Equation (1) shows the ratio of the static quadrupole moment of the 2_1^+ state to that which is predicted by the rotational model, called the reduced quadrupole moment $[Q_s(2_1^+)/Q_s^{rot}(2_1^+)]$ [25]. If the nuclear shape is axial, the value calculated for prolate will be +1, while oblate will be −1. The $Q_s(2_1^+)/Q_s^{rot}(2_1^+)$ can be used to help examine the systematics of even-even Mo isotopes in this region, as seen in panel (c) of Fig. 5. A similar entity for examining the nuclear shape in this style, $\cos(3\gamma)$, is given by Kumar and Cline to find intrinsic nuclear deformation independent of models [10,26]. When dealing with the ground state of near-axial even-even nuclei, $\cos(3\gamma)$ can be considered as approximately $Q_s(2_1^+)/Q_s^{rot}(2_1^+)$ [25,27]:

$$\frac{Q_s(2_1^+)}{Q_s^{\rm rot}(2_1^+)} = -\frac{7}{2}\sqrt{\frac{5}{16\pi}}\frac{Q_s(2_1^+)}{\sqrt{B(E2; 0_1^+ \rightarrow 2_1^+)}}. \quad (1)$$

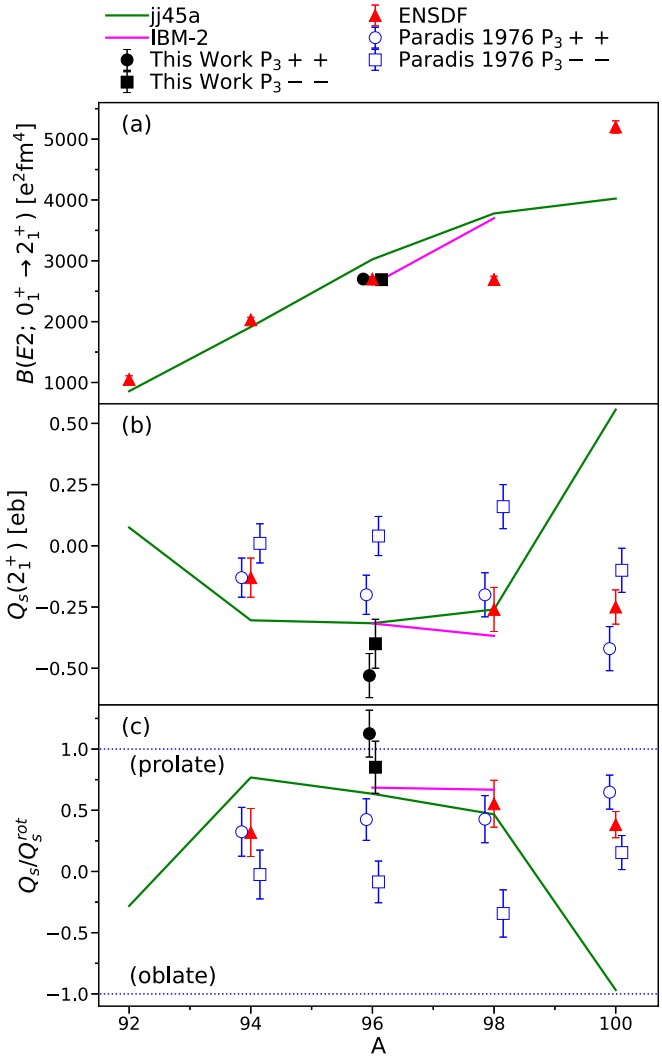

FIG. 5. $B(E2;0_1^+ \rightarrow 2_1^+)$, $Q_s(2_1^+)$, and Q_s/Q_s^{rot} for molybdenum isotopes are shown in (a), (b), and (c), respectively. Results from this work are shown in black, results from Paradis *et al.* (1976) [5] are shown with hollow blue points, and adopted experimental values from ENSDF [20] are shown with red triangles. $P_3 + +$ values are indicated by squares, $P_3 - -$ values are indicated with circles. In addition to experimental data, shell model predictions using the jj45a interaction are indicated with the green line, and the IBM-2 based calculation indicated by the magenta line. In (a) the previous work on ^{96}Mo aligns well with this work and follows the trend given using the shell model. In (b) it can be seen that values provided by the Paradis *et al.* (1976) paper [5] disagree with this work and differ somewhat from other works. In (c) this work shows a prolate deformation seen by the points being at the axially symmetric limit for prolate nuclei as outlined in Eq. (1). It is worth noting that for ^{94}Mo and ^{96}Mo, Paradis *et al.* (1976) [5] is the primary or sole contributor to the ENSDF adopted values displayed.

It is worth mentioning that in Eq. (1), the impact of effective charges is diminished due to the ratio used.

The data for the $0_1^+ \rightarrow 2_1^+$ transition and 2_1^+ state in even Mo isotopes are shown in Fig. 5. The second panel (b) in Fig. 5 contains the measurements for $Q_s(2_1^+)$ by Ref. [5], this work, and the adopted values from ENSDF [20]. The ^{92}Mo, ^{98}Mo, and ^{100}Mo data points from ENSDF use a weighted mean of data from Refs. [4,28–34] among others, with a contribution also from Ref. [5]. As opposed to the ^{94}Mo and ^{96}Mo data, which is primarily from Ref. [5]. Since there is variation in the values due to the constructive and destructive interference from intruder states, the data from Ref. [5] and this work have the values with maximum constructive and destructive components plotted (P_3 being $++$ and $--$).

The shell model reproduces $B(E2)$ experimental values well, up to ^{96}Mo, whereas ^{98}Mo and ^{100}Mo are each less well reproduced as the effects of the intruder states become significant. Regarding the $Q_s(2_1^+)$, the experimental values for Mo isotopes up to ^{98}Mo agree well with the shell model calculations. Shell-model calculations also include the 4_1^+ state with the $B(E2)$ and $Q_s(4_1^+)$ both well reproduced. The mapped IBM-2 calculations similarly predict a prolate deformation in ^{96}Mo and ^{98}Mo. As with the shell model calculations the IBM-2 model significantly overpredicts the $B(E2;0_1^+ \rightarrow 2_1^+)$ value at ^{98}Mo. We note, however, that the $2_1^+ \rightarrow 0_2^+$ decay branch in ^{98}Mo is experimentally complicated to determine due to its low energy and large internal conversion coefficient, which may contribute to this discrepancy.

Beyond the shell model and IBM-2 calculations used for comparison with this work, other theoretical studies have supported that ^{96}Mo has prolate nuclear deformation. Work by Mu *et al.* [35] using IBM-2, and Chandra *et al.* [36] using Projected Hartree-Fock-Bogoliubov (PHFB), among others also share the conclusions from this work. Both calculations point towards a modest deformation, with $\beta_2 = 0.182$ from the shell model and $\beta_2 = 0.169$ from the IBM-2 calculations. This is in good agreement with the present work, from which a $\beta_2 = 0.172$ value was determined (see Ref. [37] for β_2 definition and systematics). The calculations also agree on the sign and magnitude of both $Q_s(2_1^+)$ and $Q_s(2_1^+)/Q_s^{rot}(2_1^+)$, consistent with a prolate central deformation. We note that the present experimental data and shell model calculations can provide only approximate information regarding the degree of softness of the deformation, although the potential energy surfaces presented by Thomas *et al.* [24] indicate significant β_2 softness. Using the approximate solutions outlined in Ref. [38], we find a large degree of β_2 softness, both in the experimental data and shell-model calculations.

V. CONCLUSIONS

The measurements presented in this work show the results of safe Coulomb excitation carried out on ^{96}Mo with a ^{196}Pt target. Results presented show the first measurement of the $Q_s(4_1^+)$ for ^{96}Mo, and new measurements of $Q_s(2_1^+)$, $B(E2;0_1^+ \rightarrow 2_1^+)$, and $B(E2;2_1^+ \rightarrow 4_1^+)$. It is found that the ^{96}Mo nucleus is modestly prolate deformed, a conclusion supported by both the shell-model calculations using the jj45a interaction and the IBM and Skyrme calculation, in addition to previous theoretical work.

ACKNOWLEDGMENTS

The authors thank the beam-delivery team at the National Superconducting Cyclotron Laboratory for providing the beam. Work at the University of Surrey was supported under UKRI Future Leaders Fellowship Grant No. MR/T022264/1 and by the Science and Technologies Facilities Council (STFC). The work was supported by US DOE Contract No. 89233218CNA000001, and by the U.S. Department of Energy, Office of Science, Office of Nuclear Physics, under Contract No. DE-AC02-06CH11357 (ANL) and under Grant No. DE-SC0023633 (MSU), the US National Science Foundation (NSF) under Grant No. PHY-1565546, and by the DOE National Nuclear Security Administration through the Nuclear Science and Security Consortium, under Award No. DE-NA0003180. Work at Lawrence Livermore National Laboratory was performed under the auspices of the U.S. Department of Energy under Contract No. DE-AC52-07NA27344.

[1] T. Otsuka, Y. Tsunoda, T. Abe, N. Shimizu, and P. Van Duppen, Phys. Rev. Lett. **123**, 222502 (2019).

[2] K. Heyde and J. L. Wood, Rev. Mod. Phys. **83**, 1467 (2011).

[3] P. Singh, R. G. Pillay, J. A. Sheikh, and H. G. Devare, Phys. Rev. C **45**, 2161 (1992).

[4] K. Wrzosek-Lipska, L. Próchniak, M. Zielińska, J. Srebrny, K. Hadyńska-Klek, J. Iwanicki, M. Kisieliński, M. Kowalczyk, P. J. Napiorkowski, D. Pietak, and T. Czosnyka, Phys. Rev. C **86**, 064305 (2012).

[5] P. Paradis, G. Lamoureux, R. Lecomte, and S. Monaro, Phys. Rev. C **14**, 835 (1976).

[6] J. Barrette, M. Barrette, A. Boutard, R. Haroutunian, G. Lamoureux, G. Renaud, and S. Monaro, Nucl. Phys. A **172**, 41 (1971).

[7] E. Lunderberg, J. Belarge, P. Bender, B. Bucher, D. Cline, B. Elman, A. Gade, S. Liddick, B. Longfellow, C. Prokop, D. Weisshaar, and C. Wu, Nucl. Instrum. Methods Phys. Res. A **885**, 30 (2018).

[8] W. Mueller, J. Church, T. Glasmacher, D. Gutknecht, G. Hackman, P. Hansen, Z. Hu, K. Miller, and P. Quirin, Nucl. Instrum. Methods Phys. Res. A **466**, 492 (2001).

[9] D. Cline, H. Gertzman, H. Gove, P. Lesser, and J. Schwartz, Nucl. Phys. A **133**, 445 (1969).

[10] D. Cline, Annu. Rev. Nucl. Part. Sci. **36**, 683 (1986).

[11] S. A. Gillespie, J. Henderson, K. Abrahams, F. A. Ali, L. Atar, G. C. Ball, N. Bernier, S. S. Bhattcharjee, R. Caballero-Folch, M. Bowry, A. Chester, R. Coleman, T. Drake, E. Dunling, A. B. Garnsworthy, B. Greaves, G. F. Grinyer, G. Hackman, E. Kasanda, R. LaFleur, S. Masango, D. Muecher, C. Ngwetsheni, S. S. Ntshangase, B. Olaizola, J. N. Orce, T. Rockman, Y. Saito, L. Sexton, P. Šiurytė, J. Smallcombe, J. K. Smith, C. E. Svensson, E. Timakova, R. Wadsworth, J. Williams, M. S. C. Winokan, C. Y. Wu, and T. Zidar, Phys. Rev. C **104**, 044313 (2021).

[12] P. C. Bender, GRUTINIZER (2022), https://github.com/pcbend/GRUTinizer.

[13] R. Brun and F. Rademakers, Nucl. Instrum. Methods Phys. Res. A **389**, 81 (1997), New Computing Techniques in Physics Research V.

[14] J. Smallcome, jROOTAnalysisTools: Samuel Johnson (2020).

[15] J. Heery *et al.* (unpublished).

[16] T. Czosnyka, D. Cline, and C.-Y. Wu, Bull. Am. Phys. Soc. **28**, 745 (1983).

[17] J. F. Ziegler, M. Ziegler, and J. Biersack, Nucl. Instrum. Methods Phys. Res. B **268**, 1818 (2010).

[18] J. Henderson, GOSIAFitter (2023), https://github.com/jhenderson88/GOSIAFitter.

[19] C. Lim, R. Spear, M. Fewell, and G. Gyapong, Nucl. Phys. A **548**, 308 (1992).

[20] NNDC, Evaluated Nuclear Structure Data File (ENSDF).

[21] M. Zielińska, Low-energy coulomb excitation and nuclear deformation, in *The Euroschool on Exotic Beams*, Vol. VI, edited by S. M. Lenzi and D. Cortina-Gil (Springer International Publishing, Cham, 2022), pp. 43–86.

[22] N. Shimizu, T. Mizusaki, Y. Utsuno, and Y. Tsunoda, Comput. Phys. Commun. **244**, 372 (2019).

[23] D. Rhodes, B. A. Brown, J. Henderson, A. Gade, J. Ash, P. C. Bender, R. Elder, B. Elman, M. Grinder, M. Hjorth-Jensen, H. Iwasaki, B. Longfellow, T. Mijatović, M. Spieker, D. Weisshaar, and C. Y. Wu, Phys. Rev. C **103**, L051301 (2021).

[24] T. Thomas, V. Werner, J. Jolie, K. Nomura, T. Ahn, N. Cooper, H. Duckwitz, A. Fitzler, C. Fransen, A. Gade, M. Hinton, G. Ilie, K. Jessen, A. Linnemann, P. Petkov, N. Pietralla, and D. Radeck, Nucl. Phys. A **947**, 203 (2016).

[25] S. J. Q. Robinson, A. Escuderos, L. Zamick, P. von Neumann-Cosel, A. Richter, and R. W. Fearick, Phys. Rev. C **73**, 037306 (2006).

[26] K. Kumar, Phys. Rev. Lett. **28**, 249 (1972).

[27] J. Henderson, Phys. Rev. C **102**, 054306 (2020).

[28] P. Paradis, R. Lecomte, S. Landsberger, and S. Monaro, Phys. Rev. C **20**, 1201 (1979).

[29] K. Wrzosek-Lipska, M. Zielińska, K. Hadyńska-Klek, Y. Hatsukawa, J. Iwanicki, J. Katakura, M. Kisieliński, M. Koizumi, M. Kowalczyk, H. Kusakari *et al.*, Int. J. Mod. Phys. E **20**, 443 (2011).

[30] I. M. Naquib, A. Christy, I. Hall, M. F. Nolan, and D. J. Thomas, J. Phys. G **3**, 507 (1977).

[31] S. Mundy, W. Gelletly, J. Lukasiak, W. Phillips, and B. Varley, Nucl. Phys. A **441**, 534 (1985).

[32] M. Zielińska, T. Czosnyka, J. Choiński, J. Iwanicki, P. Napiorkowski, J. Srebrny, Y. Toh, M. Oshima, A. Osa, Y. Utsuno, Y. Hatsukawa, J. Katakura, M. Koizumi, M. Matsuda, T. Shizuma, M. Sugawara, T. Morikawa, H. Kusakari, A. Efimov, and V. Mikhajlov, Nucl. Phys. A **712**, 3 (2002).

[33] J. Barrette, M. Barrette, A. Boutard, R. Haroutunian, G. Lamoureux, and S. Monaro, Phys. Rev. C **6**, 1339 (1972).

[34] J. Lange, D. Caemmerer, C. Uhlhorn, and H. Buttlar, Nucl. Phys. A **311**, 264 (1978).

[35] C.-F. Mu and D.-L. Zhang, Chin. Phys. Lett. **35**, 062101 (2018).

[36] R. Chandra, J. Singh, P. Rath, P. Raina, and J. Hirsch, Eur. Phys. J. A **23**, 223 (2005).

[37] B. Pritychenko, M. Birch, B. Singh, and M. Horoi, At. Data Nucl. Data Tables **107**, 1 (2016).

[38] V. Werner, P. von Brentano, and R. Jolos, Phys. Lett. B **521**, 146 (2001).